A finite-element model of oxygen diffusion in the pulmonary capillaries

ANDREAS O. FRANK, C. J. CHARLES CHUONG, AND ROBERT L. JOHNSON
Biomedical Engineering Program, University of Texas at Arlington, Arlington 76019; and Department of Internal Medicine, University of Texas Southwestern Medical Center at Dallas, Dallas, Texas 75235

Frank, Andreas O., C. J. Charles Chuong, and Robert L. Johnson. A finite-element model of oxygen diffusion in the pulmonary capillaries. *J. Appl. Physiol.* 82(6): 2036–2044, 1997.—We determined the overall pulmonary diffusing capacity (D_L) and the diffusing capacities of the alveolar membrane (Dm) and the red blood cell (RBC) segments (De) of the diffusional pathway for O_2 by using a two-dimensional finite-element model developed to represent the sheet-flow characteristics of pulmonary capillaries. An axisymmetric model was also considered to assess the effect of geometric configuration. Results showed the membrane segment contributing the major resistance, with the RBC segment resistance increasing as O_2 saturation (S_{O_2}) rises during the RBC transit: RBC contributed 7% of the total resistance at the capillary inlet (S_{O_2} = 75%) and 30% toward the capillary end (S_{O_2} = 95%) for a 45% hematocrit (Hct). Both Dm and D_L increased as the Hct increased but began approaching a plateau near an Hct of 35%, due to competition between RBCs for O_2 influx. Both Dm and D_L were found to be relatively insensitive (2~4%) to changes in plasma protein concentration (28~45%). Axisymmetric results showed similar trends for all Hct and protein concentrations but consistently overestimated the diffusing capacities (~2.2 times), primarily because of an exaggerated air-tissue barrier surface area. The two-dimensional model correlated reasonably well with experimental data and can better represent the O_2 uptake of the pulmonary capillary bed.

finite-element method modeling; hematocrit; plasma protein concentration

OXYGEN UPTAKE WITHIN THE LUNGS, from the alveolar air space to a heme-binding site on a hemoglobin molecule inside of a red blood cell (RBC), is dictated by the diffusion characteristics of this pathway and the chemical reactions within the RBC. Conceptually, the total resistance for the oxygen uptake in this pathway ($1/D_L$, where D_L is lung diffusing capacity) can be expressed as the algebraic sum of that, due to a membrane segment ($1/Dm$, where Dm is membrane diffusing capacity) and an RBC segment [$1/(\theta \cdot Vc)$, where θ is the specific rate of gas uptake by RBCs and Vc is the pulmonary capillary blood volume]. This was originally defined by the Roughton and Forster equation (18) written as

$$\frac{1}{D_L} = \frac{1}{Dm} + \frac{1}{\theta \cdot Vc} \qquad (1)$$

where the apparent D_L is in $ml \cdot min^{-1} \cdot mmHg^{-1}$, Dm is in $ml \cdot min^{-1} \cdot mmHg^{-1}$, θ in blood with a normal hematocrit (Hct) is in $ml \cdot min^{-1} \cdot mmHg^{-1} \cdot ml\ blood^{-1}$, and Vc is in ml. The product of θ and Vc is referred to as the RBC diffusing capacity (De). The diffusive transport across the membrane segment, which accounts for both the blood-gas tissue barrier and the plasma fluid, can be mathematically described as a simple passive diffusion process. However, oxygen transport within the RBC segment involves passive diffusion of oxygen, as well as binding of oxygen to hemoglobin and diffusion of oxyhemoglobin, i.e., facilitated diffusion of oxygen.

The lumped-parameter representation of *Eq. 1* was a conceptual milestone, which allowed Dm and Vc to be quantified from experimental determination of D_L for CO at different oxygen tensions (18). Such data could be translated into oxygen diffusing capacities. *Equation 1*, however, does not address the spatially distributed nature of the oxygen gas transport process. Federspiel (8) applied a finite-difference numerical method to calculate the D_L by assuming spherical RBCs uniformly spaced inside a cylindrical capillary tube. However, capillaries in the lung are sandwiched between sheets of alveolar membrane as described by sheet flow (9); thus the capillary tube configuration may not accurately reflect the air-tissue barrier across which gas transport must occur in the lungs and may lead to an overestimation of diffusing capacities. Wang and Popel (22) studied the oxygen release in the systemic microcirculation using a finite-element model considering various RBC shapes. Both studies considered the transient diffusion of oxygen and oxyhemoglobin within the RBC coupled with the chemical reaction between oxygen and hemoglobin.

In this paper, we present a model based on the finite-element method (FEM) that describes the transient oxygen transport in the pulmonary capillaries from the alveolar air space to the RBCs. We considered a modified two-dimensional (2D) geometry with parachute-shaped RBCs in a parallel-sided channel, which incorporates the available surface area at the air-tissue barrier and the RBC wall. This modified 2D geometry was used to represent the sheet-flow configuration of the pulmonary capillaries (9). To assess the effects of the capillary geometry, an axisymmetric model was also considered. The contributions to the diffusional

resistance imposed by the membrane and RBC segments were determined and expressed as their respective diffusing capacities; from these, the total diffusing capacity was calculated. Effects of varying Hct and varying plasma protein concentrations on diffusive transport were also examined.

METHODS

Geometric model of a typical capillary segment. A modified 2D model with parachute-shaped RBCs in a parallel-sided channel was used to represent the sheet-flow characteristics (9) of pulmonary capillary blood flow. The model incorporated the available surface area for gas transport at the air-tissue barrier and the RBC wall. The model geometry consists of a cross section through the longitudinal axis of a typical pulmonary capillary segment (100 μm length) containing a variable number of equally spaced RBCs depending on the segmental Hct (Fig. 1*A*).

The parachute shape of the RBC was digitized from a photograph of Skalak and Branemark (20), fitted with cubic splines, and then used as the cross section for all the RBCs in the capillary segment (Fig. 1*A*). Human RBCs are known to have a mean volume of ~97 μm^3 and a mean surface area of ~137 μm^2 (10), and it is important to incorporate these values into the model, since they can greatly affect the amount of transient gas transport. The 2D planar model was thus modified to have an effective depth of 4.92 μm, resulting in an RBC volume of 103 μm^3 and an effective surface area of 125 μm^2. Note that the effective surface area considers only that which is used for gas transport at the RBC perimeter along the peripheral surface and does not include the area of the front or back faces of the RBC.

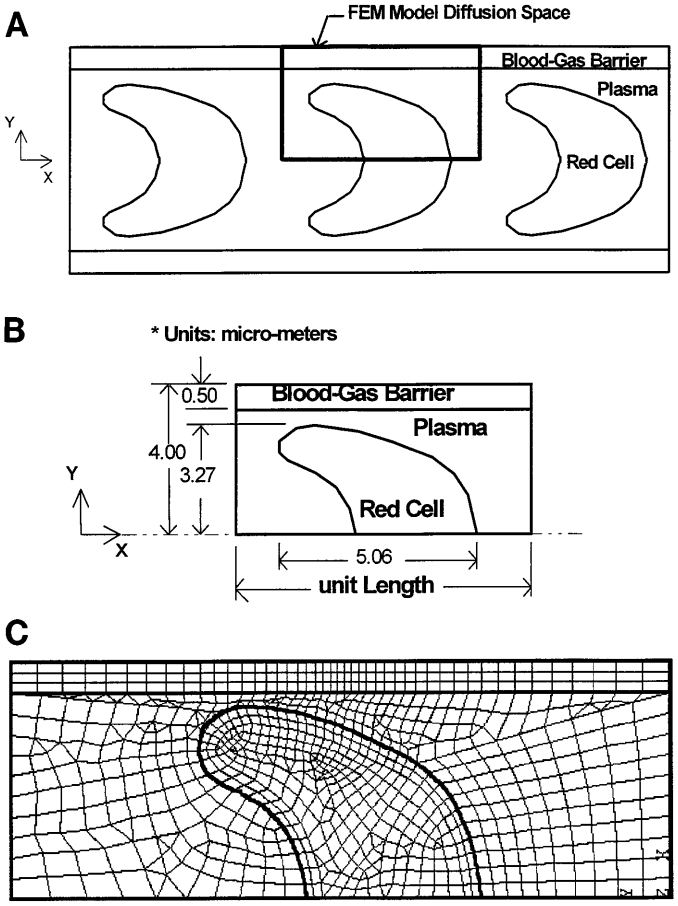

Fig. 1. A 2-dimensional (2D) model consisting of parachute-shaped red blood cells (RBCs) in a parallel-sided channel (100 μm) was used to represent sheet-flow characteristics (see Ref. 9) in alveolar septum. *A*: geometric model of a pulmonary capillary segment with 3 "unit length" segments containing 3 RBCs. *B*: respective geometric dimensions where unit length is adjusted to account for varying hematocrit (Hct) values. *C*: a typical finite-element mesh. Note that the same shape is used in axisymmetric configurations with *y*-axis representing radial direction. FEM, finite-element model.

Assuming that the RBCs are equally distributed within a pulmonary capillary bed, we can study the oxygen diffusion characteristics by examining a typical unit segment, i.e., one RBC in its surrounding tissue-plasma barrier and the alveolar air. Additionally, we have taken advantage of the symmetry with respect to the *x*-axis and only modeled one-half of such a typical unit segment (Fig. 1*A*). Therefore, the model consists of three different regions (Fig. 1*B*): *1*) the blood-gas tissue barrier, *2*) the plasma fluid within the capillary, and *3*) the RBC, each with respective gas-diffusive properties. The effect of varying Hct was studied by adjusting the "unit length" of the capillary segment, which effectively changes the volume of plasma fluid but does not alter the volume of the RBC within the capillary segment (Fig. 1*B*). In this study, the Hct was varied from 10 to 50% by increments of 5%.

Axisymmetric representation. By using the same shape as the 2D model (Fig. 1*B*), an axisymmetric model was also constructed so that the effects of capillary geometry could be assessed. Specifically, the differences in diffusing-capacity parameters could be evaluated, resulting from differences in the surface area available for gas transport and geometric shape factors. For the axisymmetric model, the *y*-axis is now interpreted as the radial direction (Fig. 1, *A* and *B*). As with the 2D planar configuration, the unit length of the diffusion space was adjusted to simulate the effect of varying Hct. All of the radial dimensions were maintained to be the same as those in the 2D model to allow for a direct comparison of the geometric configurations. The resulting volume and the surface area of the RBCs for the axisymmetric case were 103 μm^3 and 133 μm^2, respectively.

Passive diffusion in the membrane segment. Due to the low Peclet number in pulmonary capillary blood flow, we have neglected the convective transport (1, 8, 13). When a reference frame moving with the RBC is used and the differences in the plasma fluid and RBC traveling speed are neglected, the passive diffusive transport in the membrane segment (blood-gas barrier and plasma fluid) can be described by a simple diffusion process written as

$$\alpha \frac{\partial P_{O_2}}{\partial t} = \alpha d_{O_2} \nabla^2 P_{O_2} \qquad (2)$$

where t is time, ∇^2 is the Laplace operator ($= \partial^2/\partial x^2 + \partial^2/\partial y^2 + \partial^2/\partial z^2$), α is the solubility coefficient for oxygen (assumed to be constant), and d_{O_2} is the diffusion coefficient for oxygen.

Facilitated diffusion within the RBC segment. The diffusive transport inside the RBC is described by a more complicated facilitated diffusion due to the oxygen and hemoglobin interaction. Under typical conditions in the microcirculation, the facilitated diffusion can increase the rate of oxygen transport almost twofold (13). Thus the passive diffusion of oxygen, the passive diffusion of oxyhemoglobin, and the reaction between oxygen and hemoglobin must be considered, which can be written as

$$\alpha \frac{\partial P_{O_2}}{\partial t} = \alpha d_{O_2} \nabla^2 P_{O_2} + \left(\alpha \frac{\partial P_{O_2}}{\partial t} \right)_{\text{generation}} \qquad (3)$$

$$[\mathrm{Hb}]\frac{\partial S_{O_2}}{\partial t} = [\mathrm{Hb}]\, d_{\mathrm{Hb}}\nabla^2 S_{O_2} + \left\{[\mathrm{Hb}]\frac{\partial(S_{O_2})}{\partial t}\right\}_{\text{generation}} \quad (4)$$

where S_{O_2} denotes the oxygen saturation, [Hb] the total hemoglobin concentration, and d_{Hb} the diffusion coefficient for hemoglobin. Both *Eqs. 3* and *4* include generation terms accounting for the transient changes of oxygen and oxyhemoglobin due to the chemical reaction. Assuming instantaneous equilibrium for the oxyhemoglobin reaction (23), we can combine *Eqs. 3* and *4* into one equation written as

$$\alpha\frac{\partial P_{O_2}}{\partial t} + [\mathrm{Hb}]\frac{\partial S_{O_2}}{\partial t} = \alpha d_{O_2}\nabla^2 P_{O_2} + [\mathrm{Hb}]\, d_{\mathrm{Hb}}\nabla^2 S_{O_2} \quad (5)$$

with P_{O_2} and S_{O_2} governed by the Hill equation. Equivalently, the diffusive transport within the RBC can be written as

$$\left([\mathrm{Hb}]\frac{dS_{O_2}}{dP_{O_2}} + \alpha\right)\frac{\partial P_{O_2}}{\partial t} = \left([\mathrm{Hb}]\, d_{\mathrm{Hb}}\frac{dS_{O_2}}{dP_{O_2}} + \alpha d_{O_2}\right)\nabla^2 P_{O_2} \quad (6)$$

where dS_{O_2}/dP_{O_2} is the differential form of the Hill equation written as

$$\frac{dS_{O_2}}{dP_{O_2}} = \frac{n\,(P_{50})^n\,(P_{O_2})^{n-1}}{(P_{50}{}^n + P_{O_2}{}^n)^2} \quad (7)$$

with P_{50} denoting the P_{O_2} at 50% oxyhemoglobin saturation. In the present work, considering normal human blood at 37°C and pH = 7.4, the empirically derived constants of P_{50} (= 26 mmHg) and n (= 2.7) were used. Note that the diffusion of oxygen within the RBC is now represented by a single partial differential equation with nonlinear coefficients and one primary unknown (*Eq. 6*). Unlike the membrane segment, which is governed by a linear equation (*Eq. 2*), the RBC segment is described with nonlinear "diffusive properties," which need to be updated at different time steps to account for the effect of oxyhemoglobin interaction.

The assumption of instantaneous equilibrium within the RBC is valid as long as the speed of the chemical reaction greatly exceeds that for the diffusive transport. This assumption, however, must break down just inside of the RBC membrane, since the hemoglobin molecule is impermeable to the membrane, whereas oxygen is permeable. The region where deviation from equilibrium occurs has been shown to be only a thin layer inside of the RBC membrane, with the layer thickness varying depending on both spatial position along the membrane and temporal position during the RBC transit (22); i.e., Wang and Popel reported extreme cases for deviations in S_{O_2} of 10 and 4% at radial positions from the RBC membrane of 4 and 8% of the capillary radius, respectively. Because this thin layer only constitutes a small fraction of the RBC volume and becomes smaller as the RBC transit time decreases (22), the effects on the volume-weighted RBC P_{O_2} averaged over the entire transient have been neglected in the present work.

Initial and boundary conditions. The initial conditions require that the oxygen distribution (P_{O_2}) for the entire domain be prescribed. This was established by a preliminary steady-state analysis (at $t = 0$) for the entire domain with the following boundary conditions

$$P_{O_2}(t = 0, \{X, Y\}_{\text{at the air-tissue barrier}}) = 100\ \text{mmHg}$$

$$P_{O_2}(t = 0, \{X, Y\}_{\text{at the RBC surface and interior}}) = 40\ \text{mmHg}$$

Thus the initial P_{O_2} inside the RBC entering the pulmonary capillary segment was assumed to be uniform at 40 mmHg (23). The boundary conditions were maintained for the entire transient at

$$P_{O_2}(t, \{X, Y\}_{\text{at the air-tissue barrier}}) = 100\ \text{mmHg}$$

i.e., the alveolar oxygen tension was assumed to be constant at 100 mmHg throughout the entire transient, considering that there is adequate stirring in the alveolar air space. Additionally, periodic boundary conditions were imposed by forcing the P_{O_2} distribution to match at the left and right edges of the unit length (Fig. 1, *A* and *B*) as

$$P_{O_2}(t, \{X, Y\}_{\text{at the left edge}}) = P_{O_2}(t, \{X, Y\}_{\text{at the right edge}})$$

It should be noted that the P_{O_2} distribution is continuous across the RBC-plasma interface. For the axisymmetric case, the coordinate pairs $\{X, Y\}$ are understood to be $\{X, R\}$ in the above initial and boundary conditions.

Discretized FEM model and solution method. The diffusive transport for the membrane segment (blood-gas barrier and plasma regions) is governed by *Eq. 2*, whereas for the RBC segment it is governed by *Eq. 6*. The physical properties used for each different region of the model are summarized in Table 1. With isoparametric formulation, a typical discretized FEM model consists of ~500 bilinear elements with nodal P_{O_2} as the primary degree of freedom (Fig. 1*C*). For temporal discretization, a time step of 2 ms was used for the first 100 ms, followed by a time step of 4 ms for the next 200 ms of the analysis. The total transient analysis was run for 300 ms.

Governing *Eqs. 2* and *6* were solved by using the Newton-Raphson iteration technique, with the time transient portion solved by applying the general form of the trapezoid rule (2). The analysis is to find, at each time step, the P_{O_2} distribution at all nodal points that satisfy both the initial and boundary conditions. The FEM software ANSYS 5.0A (Swanson Analysis System, Houston, PA) running on a DECstation 5000 was used for the analysis.

Calculation of D_L, Dm, and De. Through the transient, at each time step, the distribution of oxygen flux was calculated from

$$O_2\ \text{flux} = \alpha d_{O_2}\frac{\partial P_{O_2}}{\partial n} \quad (8)$$

once the P_{O_2} distribution was determined, where $\partial P_{O_2}/\partial n$

Table 1. *Physical properties used in the FEM model*

Parameter	Value	Units	Source (Ref. No.)
Blood-gas barrier			
α_{O_2}	1.4	$\text{nmol}\cdot\text{cm}^{-3}\cdot\text{mmHg}^{-1}$	8
d_{O_2}	2.4×10^{-5}	cm^2/s	8
Plasma			
α_{O_2}	1.4	$\text{nmol}\cdot\text{cm}^{-3}\cdot\text{mmHg}^{-1}$	8
d_{O_2} for protein level			
Low (5 g/100 ml)	2.49×10^{-5}	cm^2/s	24
Average (6.9 g/100 ml)	2.40×10^{-5}	cm^2/s	24
High (10 g/100 ml)	2.25×10^{-5}	cm^2/s	24
Red blood cell			
α_{O_2}	1.40	$\text{nmol}\cdot\text{cm}^{-3}\cdot\text{mmHg}^{-1}$	8
d_{O_2}	2.4×10^{-5}	cm^2/s	8
[Hb]	2.0×10^{4}	nmol/cm^3	8
d_{Hb}	1.4×10^{-7}	cm^2/s	8

FEM, finite-element model; α_{O_2}, solubility coefficient for oxygen; d_{O_2}, diffusion coefficient for oxygen; [Hb], hemoglobin concentration; d_{Hb}, diffusion coefficient for hemoglobin.

denotes P_{O_2} gradients evaluated along the local normal direction of a constant P_{O_2} surface. The total oxygen flow was obtained by summing the flow along the air-tissue barrier for all participating elements. With the total oxygen flow determined, D_L for the total capillary unit segment was calculated as

$$D_L = \text{flow}/(P_A - \overline{P}_{RBC}) \quad (9)$$

where P_A is the P_{O_2} at the air-tissue barrier and $\overline{P}_{RBC}$ is the volume-weighted mean of P_{O_2} in the RBC when it is in equilibrium with S_{O_2}. Dm for the membrane segment was calculated as

$$Dm = \text{flow}/(P_A - \overline{P}_{RBC,s}) \quad (10)$$

where $\overline{P}_{RBC,s}$ is the surface-weighted mean of P_{O_2} at the RBC membrane surface. De for the RBC segment was calculated as

$$De = \text{flow}/(\overline{P}_{RBC,s} - \overline{P}_{RBC}) \quad (11)$$

Values of $\overline{P}_{RBC}$ were determined at each time step by considering the average of nodal partial pressures weighted according to the volume associated with each node, whereas for values of $\overline{P}_{RBC,s}$ the calculation was weighted according to the surface area associated with each node. Mean values in diffusing capacity parameters $\overline{D}_L$ and $\overline{D}m$ were calculated for the analysis range of hemoglobin saturation (S_{O_2}) from 74 to 96%, approximately corresponding to the normal physiological values (23). A Fortran program was written to calculate these parameters and the specific diffusing capacities (*Eqs. 9–11*) at each time step.

Effects of plasma protein concentration changes. We examined the effect of plasma protein concentration change on D_L, Dm, and De. Three levels of plasma protein concentration (5, 6.9, and 10 gm/100 ml), all within physiological range, were considered. Their respective gas diffusion coefficients (24) are listed in Table 1. At each level of protein concentration, we determined the effect of Hct for a range of 10–50% by increments of 5%.

RESULTS

Transient values in D_L, Dm, and De. Values for De decreased during the RBC transit along the capillary because of the progressive fall in the number of reduced hemoglobin binding sites available for oxygen binding. Nevertheless, De remains relatively large throughout most of the capillary transit as compared with Dm. The transient variations for all three diffusing capacity parameters are shown as a function of increasing hemoglobin saturation (S_{O_2}) for the case of average plasma protein concentration at a Hct of 45% (Fig. 2). The value of D_L per RBC diffusion space was seen to be 24.3×10^{-11} ml·min^{-1}·mmHg^{-1} at the beginning of the transient (S_{O_2} = 75%) and became 11.3×10^{-11} ml·min^{-1}·mmHg^{-1} near the end of the transient (S_{O_2} = 95%). It should be noted that the percent contribution in the total resistance (1/D_L) from the RBC segment (1/De) was determined to be only 7% at the capillary inlet (S_{O_2} = 75%) and rising to 30% toward the end of the capillary transit (S_{O_2} = 95%). Thus the relative significance of the RBC resistance gradually increases during the RBC transit. Similar trends were obtained at all protein concentration levels and Hct values.

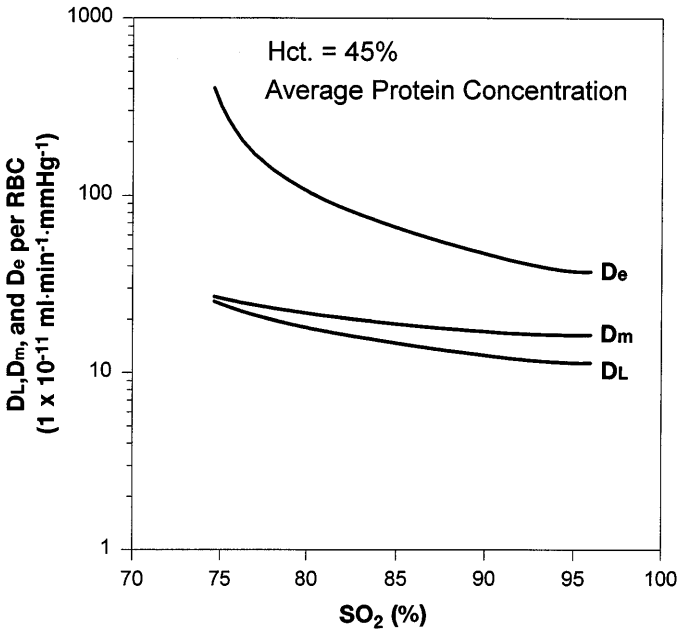

Fig. 2. Transient changes in RBC, membrane, and lung diffusing capacity parameters (De, Dm, and D_L, respectively) per RBC at varying hemoglobin saturation (S_{O_2}) (Hct, 45%; average plasma protein concentration level).

Effects of protein concentration and Hct changes. An increase in protein concentration causes a fairly uniform reduction in both Dm and D_L throughout the RBC transit, whereas a decrease in protein concentration leads to a uniform elevation (Fig. 3, *A* and *B*, for Hct = 45%). The percent changes seen in Dm and D_L due to protein concentration changes, however, were small (~2–4%) relative to the actual percent changes in protein concentration (28–45%). Similar results were obtained at all other Hct values. Results of mean diffusing capacities during the RBC transit, i.e., $\overline{D}_L$ and $\overline{D}m$ per RBC diffusion space and per 100 μm of capillary, are given in Fig. 4, *A–D*. For the average plasma protein concentration, $\overline{D}_L$ per RBC diffusion space was 17.5×10^{-11} ml·min^{-1}·mmHg^{-1} at a Hct of 10% but it decreased to 12.2×10^{-11} ml·min^{-1}·mmHg^{-1} at a Hct of 50% (Fig. 4*A*). The decrease at higher Hct is due to the competition among cells for the oxygen influx. Total $\overline{D}_L$ for the entire 100 μm capillary blood volume was seen to increase from 58.5×10^{-11} to 204×10^{-11} ml·min^{-1}·mmHg^{-1} as the Hct increased from 10 to 50%. A progressively decreasing slope is seen after 35% Hct, indicating a gradual approach toward a plateau at higher Hct values (Fig. 4*B*). Similar trends were seen for $\overline{D}m$ per RBC: it decreases from 25.8×10^{-11} to 16×10^{-11} ml·min^{-1}·mmHg^{-1} as the Hct varies from 10 to 50% because of the competition among cells (Fig. 4*C*). Total $\overline{D}m$ for the entire 100 μm capillary blood volume was seen to increase from 86.2×10^{-11} to 268×10^{-11} ml·min^{-1}·mmHg^{-1} as the Hct increased from 10 to 50%. A progressively decreasing slope is seen beyond 35% Hct, indicating a gradual approach toward a plateau (Fig. 4*D*).

Axisymmetric vs. 2D configurations. For the axisymmetric cases, the mean diffusing capacities ($\overline{D}_L$ and

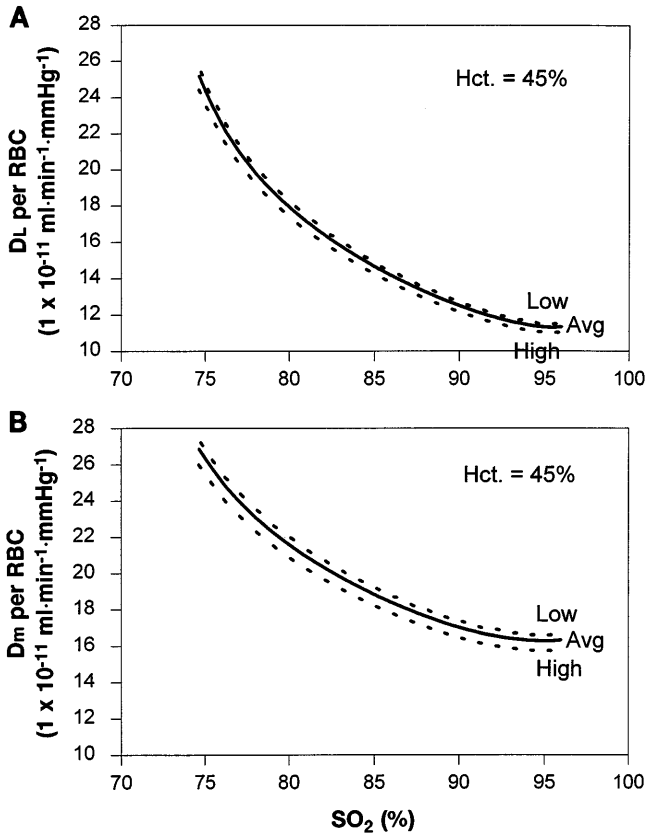

Fig. 3. Effect of plasma protein concentration level [low, average (Avg), high] on D_L and Dm per RBC at varying S_{O_2} through the transient (Hct 45%). See Table 1 for values of plasma protein concentrations. *A*: total D_L. *B*: Dm.

$\overline{D}$m) were obtained, ranging from 2.0 to 2.4 times those of their 2D planar counterparts. This was due primarily to the increased surface area available for gas transport at the air-tissue barrier with the former geometry. Further discussion on the differences between the axisymmetric and 2D cases is presented in DISCUSSION.

DISCUSSION

Variability in transient Dm and De. The progressive importance of the RBC segment in total D_L can be seen in the distribution of oxygen flux through the RBC wall membrane (Fig. 5). In an early stage of RBC transit (S_{O_2} = 75%), with the low S_{O_2} in the RBC, oxygen diffuses across the RBC membrane with little resistance. Oxygen enters the RBC most rapidly at its wall membrane closest to the capillary surface, since it is the path offering the least resistance (i.e., maximal P_{O_2} gradient). Much less flux is seen at the concave part of the RBC, which is relatively hidden from the alveolar surface. This suggests that the plasma fluid in this vicinity does not contribute to Dm and the utilization of the plasma fluid (membrane segment) is not uniform. At 85% S_{O_2}, due to the gradual increase in the relative resistance of the RBC segment with respect to the membrane segment, the distribution of oxygen flux over different regions of the RBC wall membrane becomes more uniform as compared with an S_{O_2} of 75%. Similarly, the spatial distribution of oxygen flux within the plasma becomes more uniform. Finally, at 95% S_{O_2}, total flux into the RBC becomes so low that there is no regional preference in oxygen flux through the RBC wall membrane or plasma fluid.

Thus there is a gradual progression during the RBC transit toward a more uniform distribution in the oxygen flux across the RBC wall membrane and in the utilization of the plasma fluid with respect to oxygen transport. This results in the gradual decrease in Dm (Fig. 2), since, effectively, the diffusion of oxygen from the air-tissue barrier into the RBC takes a longer path because of the increased regional resistance of the RBC. Therefore, the regional changes in De occurring throughout the transient cause the utilization of the RBC wall membrane and plasma fluid to be altered, which affects Dm.

Comparison with Dm measurements. To compare with available experimental measurements, we calculated the mean Dm at the total lung volume by using the following extrapolation

$$\overline{D}\text{m,total lung} = \text{Hct}\cdot\frac{\overline{D}\text{m,RBC}}{V_{RBC}}\cdot\text{Vc} \qquad (12)$$

where $\overline{D}$m,RBC is the mean Dm per RBC calculated by the FEM model throughout the transient, and V_{RBC} is

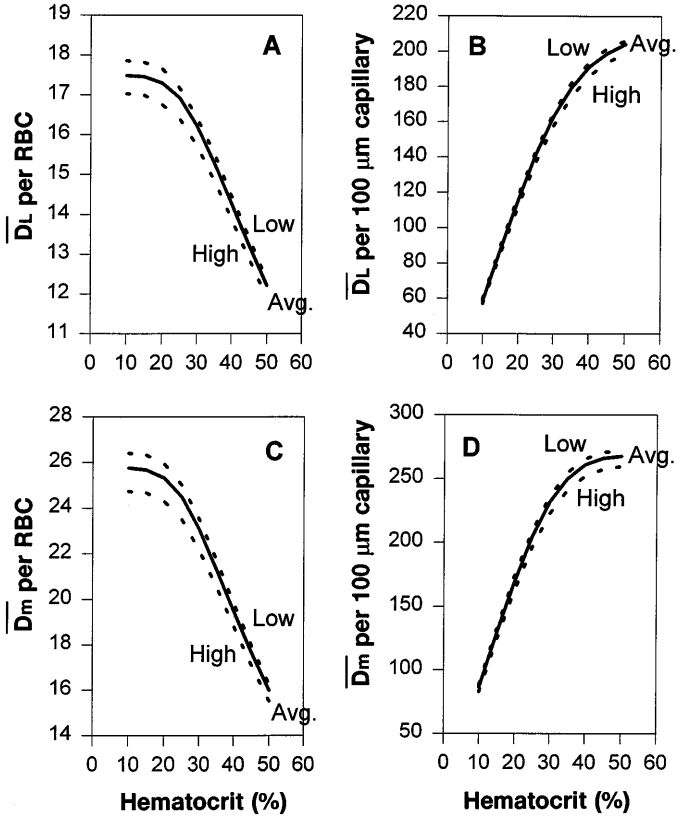

Fig. 4. Mean D_L ($\overline{D}_L$) and Dm ($\overline{D}$m) (expressed in units of 1×10^{-11} ml·min^{-1}·mmHg^{-1}) at varying Hct values for 3 different levels of plasma protein concentration. *A*: $\overline{D}_L$ per RBC. *B*: total $\overline{D}_L$ for 100 µm capillary segment. *C*: $\overline{D}$m per RBC. *D*: total $\overline{D}$m for 100 µm capillary segment.

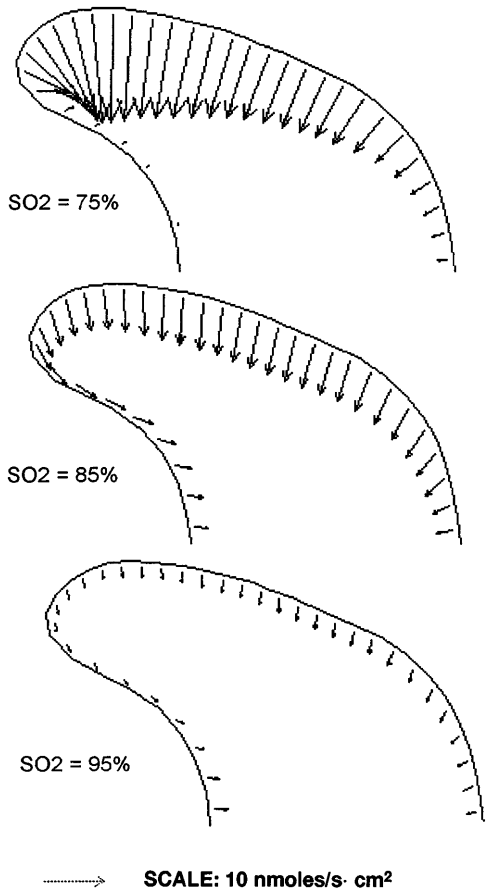

Fig. 5. Distribution of oxygen flux through RBC membrane at different stages of the transient: S_{O_2} = 75, 85, and 95% (with averaged level of plasma protein concentration at 45% Hct).

the FEM model volume of a RBC (103 μm^3). Note that $\overline{D}m,_{RBC}$ is an implicit function of Hct. Using experimentally determined data for Vc of 100.3 ml at a resting state (cardiac index ~7 l/min) and 162.8 ml at an exercise state (cardiac index ~15.5 l/min) (15), we approximated $\overline{D}m,_{total\ lung}$ for the FEM model results according to *Eq. 12*. Values in $\overline{D}m,_{total\ lung}$ were obtained at resting and exercise states for both the 2D and axisymmetric model configurations (Fig. 6). These extrapolated Dm values for the total lung showed a linear increase up to a Hct of ~35% before gradually approaching a plateau. Measurements of $Dm,_{CO}$, based on the rebreathing technique (15), were multiplied by 1.24 to yield estimated values for $Dm,_{O_2}$, shown as constant values in Fig. 6. Shaded regions represent ranges from a mean resting state of 54.1 ml·min^{-1}·mmHg^{-1}, to a moderate exercise state of 69.9 ml·min^{-1}·mmHg^{-1}, and to a peak exercise state of 115.7 ml·min^{-1}·mmHg^{-1} (15). A visual comparison indicates that the 2D planar FEM model predicted total $Dm,_{O_2}$ within a reasonable range, more so for the resting state.

Our 2D FEM model has slightly overpredicted $Dm,_{O_2}$ because it assumed an ideal condition of uniform RBC distribution and spacing within the capillaries, which offers the optimal use of the membrane segment, i.e., highest values in Dm (5). It is known that there is spatial and temporal fluctuation in both RBC distribution and spacing in the pulmonary capillary bed under physiological conditions. For the resting state, the corresponding Hct was in the range of 18–30% (Fig. 6), somewhat lower than the physiological values of 28~37% (3, 7) because of the overprediction in $Dm,_{O_2}$. For the exercise state, this source of error is further exaggerated, and the deviation in the estimated Hct is probably even larger.

2D vs. axisymmetric model. For all cases with axisymmetric configuration, mean diffusing capacities of 2.0–2.4 times their 2D counterparts were obtained. Factors contributing to the difference in diffusing capacities between geometric configurations can be separated into two categories: *1*) the available surface area for gas transport, and *2*) the geometric shape of the diffusion space. For the axisymmetric case, the available surface area at the air-tissue barrier was 2.29 times the 2D case considering the same Hct; also, there was a slightly higher RBC surface area (1.06 times). Note that the unit length (Fig. 1, *A* and *B*) for the axisymmetric case was necessarily different from the 2D so that we could match their Hct values. The increased surface area, primarily that at the air-tissue barrier, was responsible for most of the exaggerated diffusing capacity parameters. In contrast, for the axisymmetric configuration, the converging effect of the radially inward flux of oxygen would counteract the transport because

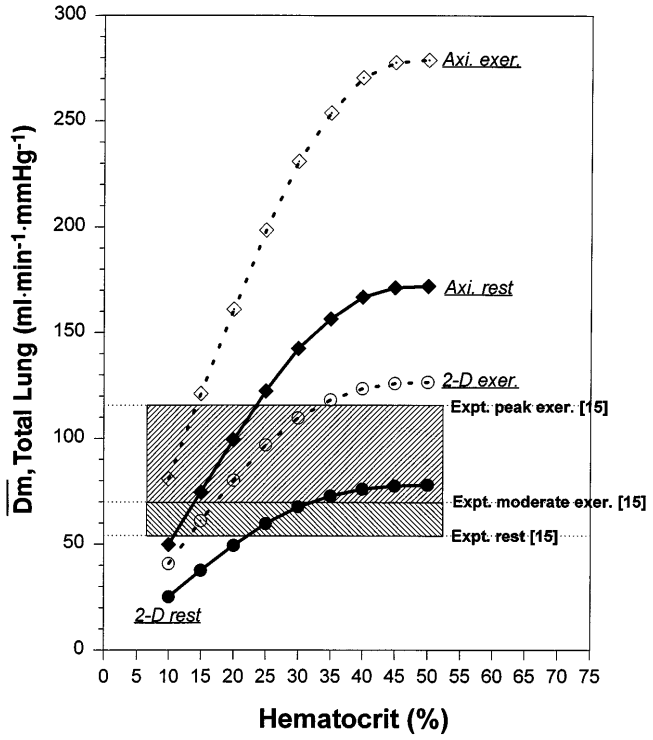

Fig. 6. Extrapolated total lung $\overline{D}m$ expressed as a function of Hct at both resting (rest) and exercise (exer) states for 2D and axisymmetric model (Axi) configurations (labeled as 2D exer, 2D rest, Axi exer, and Axi rest). Dm for oxygen derived from experimentally determined (Expt) Dm for CO shown for a range from mean resting state, moderate exercise, to peak exercise states (see Ref. 15).

of the progressively reducing area associated with the geometric shape. The effects due to geometric shape between the two configurations can be quantified in terms of Nusselt number (see below).

The calculated mean Dm values for the total lung derived from the axisymmetric cases were found to be significantly higher than the measured values, whereas the 2D cases more closely corresponded to the measurements (Fig. 6). This suggests that the 2D model is more representative of the oxygen transport in the pulmonary capillary bed. Our comparisons demonstrate that the geometric representation of the diffusion space needs to be carefully incorporated for accurate assessment of the diffusing capacity parameters.

Comparison of Nusselt numbers with other models. To compare with other mathematical models, we calculated the Nusselt number (Nu), a measure of mass transport conductance, defined as

$$\mathrm{Nu} = \frac{R_A \text{ flux}}{\alpha d_{O_2}(P_A - \overline{P}_{RBC})} \qquad (13)$$

where R_A denotes one-half of the alveolar septum thickness for the 2D case and the radius of the alveolar septum for the axisymmetric case. Calculated Nusselt numbers were added to Fig. 14 of Ref. 14 for comparison (Fig. 7*A*). It should be noted that all of these previous works on systemic microcirculation utilized cylindrically shaped diffusion spaces with an axisymmetric geometry and the values presented were for a Hct of 25% and hemoglobin saturation of 70%. They were derived to represent oxygen delivery to the tissues, as opposed to oxygen uptake by the lungs; thus the hemoglobin saturation is outside of the range represented by the present model. For comparison purposes, we calculated Nusselt numbers of the present models for a hemoglobin saturation of 75% and a Hct of 25%. The results for the present models compare reasonably with the previous works (Fig. 7*A*) (12, 16, 17, 19, 22).

The Nusselt number, written in terms of flux (flow/area), represents the ratio between the rates of actual mass transfer and the diffusive transfer. For the axisymmetric case, the Nusselt number was found to be 20% lower than its 2D counterpart at a Hct of 25%, suggesting a higher efficiency with the latter configuration, which is to mimic the sheet-flow configuration. Note that the greater diffusing capacity parameters (~2.2 times) for the axisymmetric configuration are primarily due to its exaggerated surface area at the air-tissue barrier. Effect of surface area is removed in the calculation of Nusselt number, since it is based on flux and not flow (flux × area). Thus the differences in Nusselt number between the axisymmetric and 2D cases are due to the converging effect with the former, i.e., oxygen molecules are competing for the progressively reducing surface area available.

As with the diffusing capacity parameters, the Nusselt number from the present work is seen to be strongly dependent on Hct. Calculated mean Nusselt

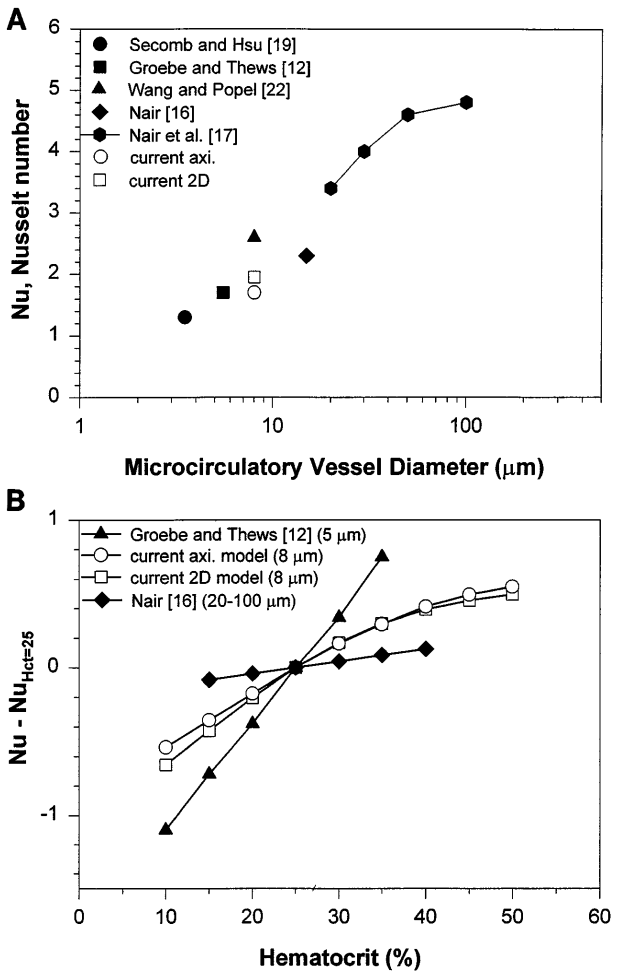

Fig. 7. *A*: Nusselt numbers (Nu) calculated at different vessel diameters, adapted from Fig. 14 of Hellums et al. (14). Data from previous work are for oxygen release to tissues calculated at 25% Hct and 70% hemoglobin saturation; whereas data from present model are for oxygen uptake by lungs also calculated at 25% Hct and 75% hemoglobin saturation. Note that these previous models consider axisymmetric capillaries, whereas present model considers both 2D and axisymmetric configurations. *B*: Nu as a function of Hct for various capillary vessel diameters. Note that Nu are expressed in terms of $(\mathrm{Nu} - \mathrm{Nu}_{\mathrm{Hct}=25})$ to facilitate comparison.

numbers in terms of $\mathrm{Nu} - \mathrm{Nu}_{\mathrm{Hct}=25}$ were plotted as a function of Hct with data from previous works (12, 16) in Fig. 7*B*. They reveal the dependency of the Nusselt number on Hct for various-sized capillaries. The data from Groebe and Thews (12), based on oxygen delivery with axisymmetric capillaries of a 5.5-μm diameter, show a stronger dependency on Hct as compared with the present models (capillary diameter of 8 μm). On the other hand, data from Nair (16) represent larger vessel diameters (20–100 μm), showing a much smaller dependency on Hct. These comparisons suggest that the Nusselt number (oxygen mass transfer conductance) becomes more strongly dependent on Hct as the capillary vessel size decreases, and for small capillary vessels the Hct can have a significant effect on oxygen transport.

Comparison with RBC conductance θ. Using the mean $\overline{D}e$ per RBC throughout the entire transient, we

calculated an equivalent θ value of 5.9 $ml \cdot min^{-1} \cdot mmHg^{-1} \cdot ml$ whole $blood^{-1}$ for an Hct of 45%. This was obtained on the assumption of infinite reaction velocity between oxygen and hemoglobin. To calculate it, we have considered a transient analysis from 0 to 80% S_{O_2} to simulate the experimental conditions of rapid-reaction techniques (21, 24), which indicated nearly constant θ values for this S_{O_2} range. Above 80% saturation, the RBC conductance θ progressively falls as the saturation rises due to the progressive decrease in the number of binding sites provided by the last heme on the hemoglobin molecule (21). Measured values of θ have been reported to be 2.8 (21) and 3.8 $ml \cdot min^{-1} \cdot mmHg^{-1} \cdot ml$ whole $blood^{-1}$ (24). However, the rapid-reaction technique may never completely eliminate the unstirred plasma layer around the RBC and, hence, tends to underestimate the θ value; whereas the present work tends to overestimate the θ value due to the assumed infinite reaction velocity.

Neglect of convective diffusion. Our model neglected convective diffusion of oxygen within the pulmonary capillary. This assumption was made with the consideration that the effect of convective diffusion is small compared with that of conductive diffusion. Two possible mechanisms could contribute to the convective diffusion within the capillary bed: *1*) relative motion between the RBC and the blood plasma, and *2*) relative motion between the RBC membrane and its interior contents.

Convection due to the former mechanism would lead to increased oxygen conductance of the membrane segment, which could reduce the role of the membrane segment as the limiting resistance of the pulmonary diffusion process (13). Flow velocity at capillary is relatively low (~0.2 cm/s), with a low Reynolds number (~0.001) (4). The relative motion of plasma fluid with respect to the RBC, particularly that at the cell-endothelial gap, is known to be nonuniform with a complex circulating pattern associated with the propulsion of the RBCs (4). The plasma fluid moves at a speed lower than that of the RBC as a consequence of the no-slip velocity boundary condition at the capillary wall. With an effective Peclet number of <1 (8), the enhanced mixing due to the stirring motion in plasma should not appreciably affect the diffusive transport of dissolved gasses such as oxygen (1), especially for higher Hct values (13).

The second mechanism considers the relative motion between the RBC membrane and the cytoplasm within, known as "tank treading" (11). It occurs within the RBC segment of the diffusion space and would thus tend to increase the RBC conductance. An increase of the RBC conductance would tend to decrease its effect on either D_L or Dm, due to its already relatively high value.

Summary. We determined diffusing capacities (D_L, Dm, and De) for oxygen using a 2D FEM, developed to represent the sheet-flow configuration of pulmonary capillaries. Results showed the membrane segment contributing the major resistance, with the RBC segment resistance increasing as S_{O_2} rises during the RBC transit. Both Dm and D_L increased as the Hct was increased but gradually approached a plateau as the Hct exceeded 35%. Both Dm and D_L were found to be relatively insensitive to changes in plasma protein concentration. Axisymmetric results showed similar trends to the 2D model for all Hct and plasma protein concentrations but consistently overestimated the diffusing capacities by ~2.2 times, primarily due to the exaggerated air-tissue barrier surface area. The 2D model correlated reasonably well with experimental data and can better represent the oxygen uptake at the pulmonary capillary bed.

The authors thank the reviewers for very constructive comments and suggestions.

This work was supported in part by National Heart, Lung, and Blood Institute Grant T32HL-07362 and by National Science Foundation Grant BCS-9008455.

Address for reprint requests: C. J. C. Chuong, Biomedical Engineering Program, PO Box 19138, 501 W 1st St., EL-220, Univ. of Texas at Arlington, Arlington TX 76019.

Received 22 March 1996; accepted in final form 14 February 1997.

REFERENCES

1. **Aroesty, J., and J. F. Gross.** Convection and diffusion in the microcirculation. *Microvasc. Res*. 2: 247–267, 1970.
2. **Bathe, K.** *Finite Element Procedures in Engineering Analysis*. Englewood Cliffs, NJ: Prentice-Hall, 1982.
3. **Brudin, L. H., S. O. Valind, C. G. Rhodes, D. R. Truton, and J. M. B. Hughes.** Regional lung hematocrit in human using positron emission tomography. *J. Appl. Physiol.* 60: 1155–1163, 1986.
4. **Caro, C. G., T. J. Pedley, R. C. Schroter, and W. A. Seed.** *The Mechanics of the Circulation*. New York: Oxford Univ. Press, 1978.
5. **Chuong, C. J. C., and R. L. Johnson, Jr.** Role of hematocrit in diffusive gas transport in lung: importance of red blood cell spacing and shape. In: *Proc. 14th Annu. Houston Conf. on Biomedical Engineering Res. Feb 8–9, 1996*, p. 98. (Also presented at the 1995 Am. Thoracic Soc. Meeting, Seattle, WA, May 20–24, 1995.)
6. **Clark, A., Jr., W. J. Federspiel, P. A. A. Clark, and G. R. Cokelet.** Oxygen delivery from red cells. *Biophys. J*. 47: 171–181, 1985.
7. **Dupuis, J., C. A. Goresky, J. L. Rouleau, G. G. Bach, A. Simard, and A. J. Schwab.** Kinetics of pulmonary uptake of serotonin during exercise in dogs. *J. Appl. Physiol.* 80: 30–46, 1996.
8. **Federspiel, W. J.** Pulmonary diffusing capacity: implications of two-phase blood flow in capillaries. *Respir. Physiol.* 77: 119–134, 1989.
9. **Fung, Y. C.** *Biomechanics: Motion, Flow, Stress, and Growth*. New York: Springer-Verlag, 1992.
10. **Fung, Y. C.** *Biomechanics: Mechanical Properties of Living Tissues* (2nd ed.). New York: Springer-Verlag, 1993.
11. **Gaehtgens, P.** Distribution of flow and red cell flux in the microcirculation. *Scand. J. Clin. Lab. Invest. Suppl*. 156: 83–87, 1981.
12. **Groebe, K., and G. Thews.** Theoretical analysis of oxygen supply to contracted skeletal muscle. *Adv. Exp. Med. Biol.* 200: 495–514, 1986.
13. **Groebe, K., and G. Thews.** Effects of red cell spacing and red cell movement upon oxygen release under conditions of maximally working skeletal muscle. *Adv. Exp. Med. Biol.* 248: 175–185, 1989.
14. **Hellums, J. D., P. K. Nair, N. S. Huang, and N. Ohshima.** Simulation of intraluminal gas transport processes in the microcirculation. *Ann. Biomed. Eng.* 24: 1–24, 1996.
15. **Hsia, C. C. W., D. G. McBrayer, and M. Ramanathan.** Reference values of pulmonary diffusing capacity during exercise

by a rebreathing technique. *Am. J. Respir. Crit. Care Med.* 152: 658–665, 1995.
16. **Nair, P. K.** *Simulation of Oxygen Transport in Capillaries* (PhD thesis). Houston, TX: Rice University, 1988.
17. **Nair, P. K., J. D. Hellums, and J. S. Olson.** Prediction of oxygen transport rates in blood flowing in large capillaries. *Microvasc. Res.* 38: 269–285, 1989.
18. **Roughton, F. J. W., and R. E. Forster.** Relative importance of diffusion and chemical reaction rates in determining rate of exchange of gases in the human lung, with special reference to true diffusing capacity of pulmonary membrane and volume of blood in the lung capillaries. *J. Appl. Physiol.* 11: 290–302, 1957.
19. **Secomb, T. W., and R. Hsu.** Simulation of O_2 transport in skeletal muscle: diffusive exchange between arterioles and capillaries. *Am. J. Physiol.* 267 (*Heart Circ. Physiol.* 36): H1214–H1221, 1994.
20. **Skalak, R., and P. T. Branemark.** Deformation of red blood cells in capillaries. *Science* 164: 717–719, 1969.
21. **Staub, N. C., J. M. Bishop, and R. E. Forster.** Velocity of O_2 uptake by human red cells. *J. Appl. Physiol.* 16: 511–516, 1961.
22. **Wang, C. H., and A. S. Popel.** Effect of red blood cell shape on oxygen transport in capillaries. *Math. Biosci.* 116: 89–110, 1993.
23. **West, J.** *Respiratory Physiology*. Baltimore, MD: Williams & Wilkins, 1975.
24. **Yamaguchi, K., D. Nguyen-Phu, P. Scheid, and J. Piiper.** Kinetics of O_2 uptake and release by human erythrocytes studied by a stopped-flow technique. *J. Appl. Physiol.* 58: 1215–1224, 1985.